ELSEVIER

Biochimica et Biophysica Acta 1418 (1999) 295–306

BIOCHIMICA ET BIOPHYSICA ACTA
BBA

Electric field-induced transient birefringence and light scattering of synthetic liposomes

N. Asgharian, Z.A. Schelly *

Department of Chemistry and Biochemistry, University of Texas at Arlington, Arlington, TX 76019-0065, USA

Received 23 September 1998; received in revised form 26 February 1999; accepted 1 March 1999

Abstract

The dynamics of electric field-induced transient birefringence $\Delta n(t)$ and light scattering (detected as turbidity) of 190 nm diameter unilamellar vesicles of dioleoylphosphatidylcholine are investigated as a function of applied field strength E, length of the square pulse Δt, lipid concentration, mean hydrodynamic diameter $\langle D_h \rangle$, ionic strength, and temperature. Generally, induced birefringence exclusively is observed at low lipid concentration and below certain threshold values of E and Δt, whereas concomitant induced turbidity appears at high lipid concentration and above thresholds values of E and Δt. Turbidity is monitored through the change in transmitted intensity $\Delta S_{\parallel}(t)$ and $\Delta S_{\perp}(t)$ of light polarized parallel and perpendicular to the applied field $\boldsymbol{E}$. The field-induced structural changes are reflected in double-exponential forward relaxation and triple-exponential reverse relaxation of the positive birefringence, and in non-exponential relaxations of $\Delta S_{\parallel}(t)$ and $\Delta S_{\perp}(t)$. Under the field, the associated physical events are interpreted as elongation of the spherical bilayer shells in the direction of $\boldsymbol{E}$, linear chain formation (pearling) of the induced dipolar liposomes parallel to $\boldsymbol{E}$, and partial fusion of adjoining vesicles within the chains. Under conditions where electroporation can be detected, pore opening succeeds the elongation of the vesicles. After termination of the field, the vesicles return to their original time average spherical shape, the oriented chains randomize and disintegrate, and the fused structures are converted either to unilamellar or multilamellar vesicles.

Keywords: Unilamellar vesicle; Unilamellar liposome; Electric birefringence; Electric light scattering; Dynamics

1. Introduction

Perturbation of organized assemblies of amphiphiles by an externally applied electric field $\boldsymbol{E}$ can provide information about the properties and dynamic behavior of such systems [1,2]. Beyond serving as a tool of investigation, the effects of electric field have also been exploited to affect desired changes such as the electroporation and electrofusion of cells and vesicles [3], to induce phase separation in water-in-oil microemulsions [4] and to reorient liquid crystals in numerous practical applications.

In the present study the forced electro-optical response of synthetic large unilamellar vesicles (LUV) to a high-voltage square pulse is investigated. The primary effect of the applied field is the polarization of the system which, above threshold values of the field strength E and pulse length Δt, leads to structurally anisotropic states of the vesicles. Structural anisotropy entails optical anisotropy, exhibited in induced birefringence $\Delta n(t)$ and induced light scattering $\Delta I_s(t)$, which are used to monitor the dynamics of the physical events involved. Early observations of elec-

* Corresponding author. E-mail: schelly@uta.edu

0005-2736/99/$ – see front matter
PII: S0005-2736(99)00042-5

tric birefringence were briefly reported for egg phosphatidylcholine (PC) and dipalmitoyl-PC vesicles in dilute buffer solutions [5], and the effects of polar and ionic fluidizing additives on the induced birefringence were investigated for vesicles of mixed lipids (egg-PC/bovine brain phosphatidylserine, 9:1) [6]. The present study was undertaken to examine the behavior of single component liposomes in the absence of any additives. Using a zwitterionic lipid (dioleoylphosphatidylcholine, DOPC) for the preparation of well-defined unilamellar vesicles, the complications associated with the presence of free ions are avoided. Through systematic variation of the experimental parameters, the effects of temperature, lipid concentration, vesicle size, ionic strength, and applied field strength and pulse length on the observed multiexponential relaxation functions are reported and discussed.

2. Materials and methods

2.1. Preparation of vesicles

Details of the preparation and characterization of the vesicles have been described elsewhere [7]. Briefly, the lipid DOPC (from Avanti Polar Lipids) was used without further purification. After evaporating the chloroform solvent, large multilamellar vesicles (MLV) were obtained by hydrating the dry lipid film in distilled and double-deionized water by vortex mixing (Vortex-2 Genie). Subsequently, the MLV suspension was extruded five times (Extruder, Lipex Biomembranes) through two stacked polycarbonate filters of suitable pore size, under nitrogen pressure of up to 3.4 atm, to produce LUVs [8]. The unilamellar nature of the DOPC vesicles ($T_c = -17.3$°C [9]) was confirmed through the extent of quenching of their ^{31}P NMR signals (Bruker MSL-300) by manganese ions [10], and their mean hydrodynamic diameter $\langle D_h \rangle$ was determined by dynamic light scattering measurements (Brookhaven Model BI-200 SM). An example of the monodisperse size distribution obtained is shown in Fig. 1.

The vesicle solutions stored at 3°C were found unchanged for 4 days as judged from the combination of repeated light scattering measurements, TLC analysis (Silica Gel 60A, K6F Whatman; mobile phase: chloroform/methanol/water 13:5:0.8 v/v/v; developed with I_2 vapor), and from the reproducibility of the transient electro-optic responses. The majority of experiments were carried out on solutions not older than 2 days.

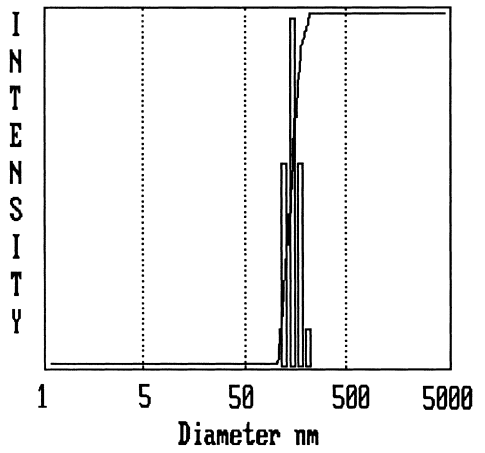

Fig. 1. Size distribution of the DOPC vesicles of mean hydrodynamic diameter $\langle D_h \rangle = 190$ nm and polydispersity = 0.078, prepared through multiple extrusion.

Due to the zwitterionic polar head group of DOPC, the vesicle solutions prepared contain no free ions originating from the surfactant. Thus, by neglecting the very low concentration of ions arising solely from the autoprotolysis of water, the ionic strength can be considered zero in all systems studied, except when the effects of the presence of electrolytes were examined.

2.2. Instrumentation

The instrument used for the electric birefringence and electric light scattering experiments has been described previously [4]. Its components are depicted in Fig. 2. The sample solution is placed between a pair of rhodium-plated stainless steel electrodes (2.5 mm apart) of the thermostated Kerr cell with an optical path length of 5 cm. The rise and fall times of the high-voltage (up to 2 kV) square pulse delivered to the electrodes are < 100 ns. A linearly polarized He-Ne laser (Melles-Griot, 10 mW TEM_{00}, $\lambda = 632.8$ nm) is used as the monitoring light source. In birefringence measurements, the Kerr cell is located between a polarizer (oriented at $\pi/4$ from the applied field $\boldsymbol{E}$) and a quarter-wave plate (the slow axis of which is at $3\pi/4$ from $\boldsymbol{E}$) followed by an analyzer (set

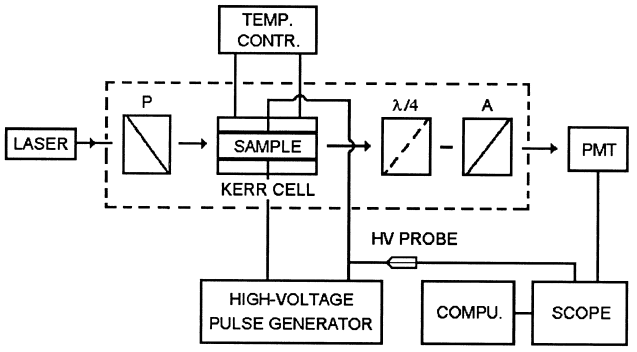

Fig. 2. Block diagram of the E-jump apparatus with birefringence detection (in dashed frame). P, polarizer; λ/4, quarter-wave plate; A, analyzer; PMT, photomultiplier tube; SCOPE, oscilloscope. For turbidity detection, the components λ/4 and A are removed.

at an angle $\pm\alpha$ relative to the quarter-wave plate), and the time dependent change of the transmitted intensity of the laser beam is recorded [11]. If induced birefringence and light scattering occur concurrently, the signal observed is the sum of birefringence and turbidity components. Conversely, light scattering alone can be detected as turbidity (i.e., loss of transmitted light intensity due to induced scattering, integrated over essentially the full solid angle) through rendering the detection system blind to birefringence by removing the quarter-wave plate and analyzer. With the plane of polarization of the incident beam set either parallel or perpendicular to the external electric field $\boldsymbol{E}$, the time dependent change of the corresponding transmitted light intensity, $\Delta S_{\parallel}(t)$ or $\Delta S_{\perp}(t)$, is monitored.

2.3. Transient electric birefringence

If birefringence occurs exclusively, the change of transmitted light intensity, $\Delta I_{\delta}(t) = I_{\delta}(t) - I_{\alpha}$, is related to the induced retardation $\delta(t)$ as

$$\frac{\Delta I_{\delta}}{I_{\alpha}} = \frac{\sin^2(\alpha + \delta/2) - \sin^2\alpha}{\sin^2\alpha} \quad (1)$$

where I_{α} is the light intensity (with the analyzer oriented at an angle α relative to the crossed position) reaching the detector in the absence of the field. The retardation yields the birefringence, $\Delta n \equiv n_{\parallel} - n_{\perp}$, through

$$\Delta n(t) = \delta(t)\lambda/2\pi l \quad (2)$$

where λ is the wavelength of the monitoring light in vacuo and l is its path length in the Kerr cell. For perturbation by a square pulse, the computed birefringence $\Delta n(t)$ consists of two parts corresponding to the forward (field-on) and reverse (field-off) relaxations (Fig. 3). The rise of the birefringence during the field-on period can be represented by a multiple exponential function of the general form

$$\Delta n(t) = \Delta n_o - \Sigma_i A_i \exp(-t/\tau_i) \quad (3)$$

and the decay of the birefringence after termination of the field can be represented by

$$\Delta n(t) = \Sigma_{-i} A_{-i} \exp(-t/\tau_{-i}) \quad (4)$$

where $A_{\pm i}$ and $\tau_{\pm i}$ are the birefringence relaxation amplitude and relaxation time of the $\pm i$th process contributing to the optical anisotropy, and Δn_o is the steady-state value of the birefringence reached under the field. In Eq. 3, $\Delta n_o = \Sigma_i A_i$.

3. Results

The experiments were carried out at 25°C and a lipid concentration $C = 0.25$ mg/ml on 190 nm diameter liposomes, unless indicated otherwise. Induced birefringence (positive) is observed above a threshold value of the applied field strength ($E \geq 0.8$ kV/cm), whereas concomitant induced turbidity occurs only if $E \geq 2$ kV/cm *and* the lipid concentration $C > 0.5$ mg/ml. Each experiment was repeated 3–4 times, and the

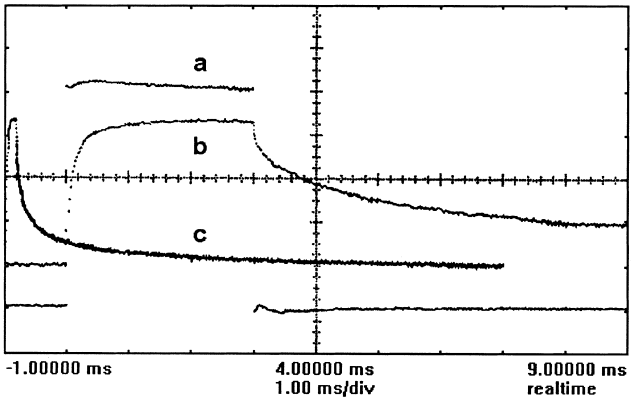

Fig. 3. Oscilloscope traces of the attenuated perturbation square pulse ($E = 4$ kV/cm, $\Delta t = 3$ ms) (a), and the electric field-induced birefringence signal of DOPC vesicles (b,c). Time scales: (a,b) 1 ms/div, (c) 20 ms/div. Trace c is the display on a slower time scale of all the data points stored for signal b.

error bars in the graphs represent standard deviation. The absence of an error bar indicates that its magnitude is comparable to or smaller than the size of the symbol used for the particular data point. To aid the eye, the data points are connected by curves generated by a spline.

3.1. Transient birefringence

The results reported were obtained under conditions where induced turbidity was absent. The field-on relaxation signal is found to be double-exponential, indicating the occurrence of at least two processes that contribute to the detectable increase of anisotropy of the system. After termination of the square pules, the birefringence decays from Δn_o back to zero according to a triple-exponential function. (The quality of fitting (χ^2) in both cases is of the order of 10^{-4}.) The overall field-off relaxation is more than an order of magnitude slower than the overall field-on relaxation. The observed dissymmetry between the forward and reverse signals indicates that the physical processes in the absence of the field are not simply the reversals of the forward processes previously induced by the electric field. In other words, the applied field is driving the system into a thermodynamic cycle that starts and ends at the original equilibrium. A similar situation was encountered in electric field perturbation studies of water-in-oil microemulsions [2,4].

3.1.1. Effects of the applied field strength

While assuring that the birefringence reaches its stead-state value Δn_o, yet to avoid the conditions under which induced turbidity becomes detectable, the pulse length Δt was successively reduced with increasing field strength E applied.

E/kV cm^{-1}	0.8	1.6	2.4	3.2	4.0	4.8	6.0	7.2
Δt/ms	7	7	6	5	5	4	3	2

Variation of the field strength reveals that the steady-state birefringence Δn_o ($=\Sigma_i A_i$) initially rises approximately linearly with E (Fig. 4), and that the system does not follow the Kerr law, $\Delta n_o = \lambda K E^2$ (where K is the Kerr constant).

The field strength dependence of the forward relaxation times τ_1 and τ_2 associated with the amplitudes A_1 and A_2 is shown in Fig. 5.

Although the triple-exponential reverse relaxation happens after termination of the perturbation, the relaxation times (τ_{-1}, τ_{-2} and τ_{-3}) and the associated amplitudes (A_{-1}, A_{-2} and A_{-3}) of the constituent

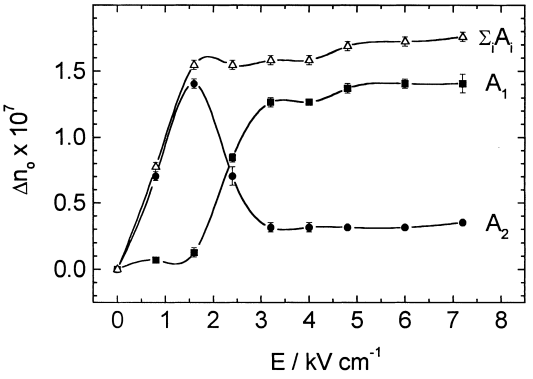

Fig. 4. Steady-state electric birefringence ($\Delta n_o = \Sigma_i A_i$) and birefringence relaxation amplitudes (A_i) of DOPC vesicles for the field-on processes as a function of the applied field strength E.

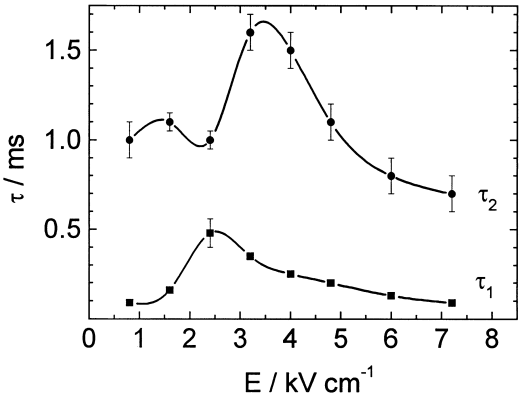

Fig. 5. Birefringence relaxation times τ_i of the field-on processes as a function of the applied field strength E.

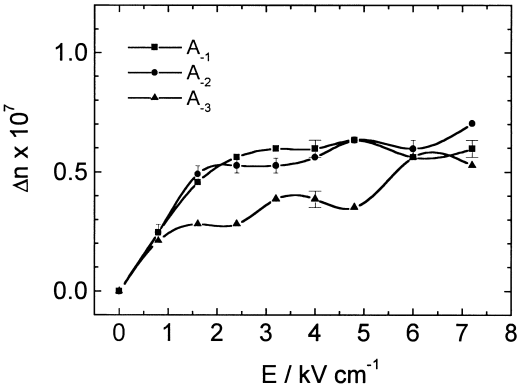

Fig. 6. Birefringence relaxation amplitudes (A_{-i}) of the field-off processes as a function of the applied field strength E.

processes can depend on the past field strength because it was the intensity and duration of the previously applied pulse that established the specific state of the system from which it has to reequilibrate. The influence of the past field strength E on A_{-i} and τ_{-i} is shown in Figs. 6 and 7.

3.1.2. Effects of pulse length

For the evaluation of the relaxation parameters of the field-on processes, the applied pulse must be long enough for the birefringence to reach steady state. Beyond this required pulse length, there is an approx. 2 ms additional period for the variation of the pulse length (up to and including the particular values of Δt listed in Section 3.1.1) which leaves the relaxation times and amplitudes of both the forward and reverse processes unaffected. For $E \geq 4$ kV/cm, *and* with pulses longer than those listed, anomalous reverse relaxations were observed, with overall reequilibration time of tens of minutes. The nature and dynamics of these processes require further investigation, and will not be discussed in the present paper. With the application of pulses shorter than necessary for the birefringence to reach steady state, the field-off relaxation times are found shorter than those obtained otherwise.

3.1.3. Effects of temperature

The influence of temperature on the relaxation parameters was examined by comparing the results obtained at 15°C and 35°C, using 2–3 ms long 4 kV/cm pulses. Increasing the temperature by 20°C has the following effects.

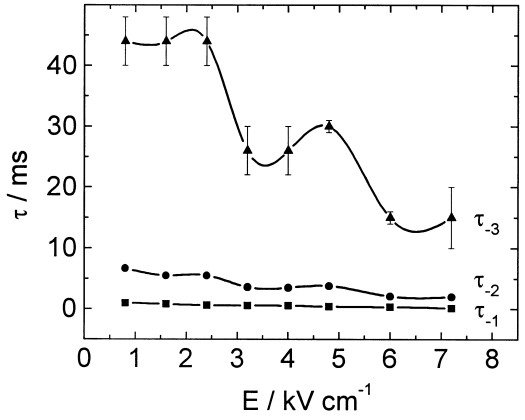

Fig. 7. Birefringence relaxation times τ_{-i} of the field-off processes as a function of the applied field strength E.

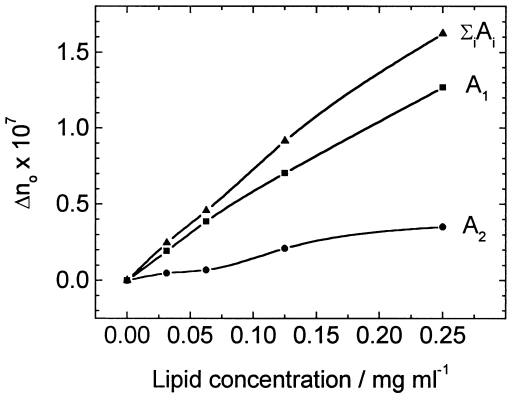

Fig. 8. Steady-state electric birefringence ($\Delta n_o = \Sigma_i A_i$) and birefringence relaxation amplitudes (A_i) of the field-on processes as a function of the lipid concentration. $E = 4$ kV/cm, $\Delta t = 4$ ms.

(i) All rate processes speed up by various degrees, i.e., the relaxation times become smaller by the indicated factors: 0.6 ± 0.05 for τ_1, 0.77 ± 0.1 for τ_2, 0.64 ± 0.06 for τ_{-1}, 0.69 ± 0.04 for τ_{-2}, and 0.68 ± 0.08 for τ_{-3}. From these, the activation energies of the individual processes can be estimated (in kJ mol^{-1}) as 18.8, 9.6, 16.5, 13.7, and 14.2, respectively.

(ii) Only the amplitudes of the fastest of the forward and reverse processes, A_1 and A_{-1}, increase (by a factor of 1.1 ± 0.03 and 1.3 ± 0.13, respectively), while all the other amplitudes decrease (by a factor of 0.61 ± 0.04 for A_2, 0.94 for A_{-2}, and 0.9 for A_{-3}).

3.1.4. Effects of lipid concentration

Since induced turbidity interferes with the birefrin-

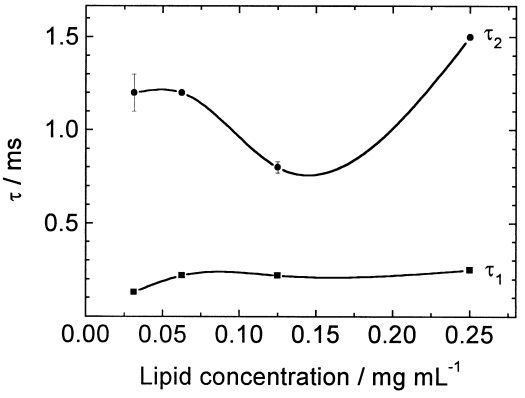

Fig. 9. Birefringence relaxation times τ_i of the field-on processes as a function of the lipid concentration. $E = 4$ kV/cm, $\Delta t = 4$ ms.

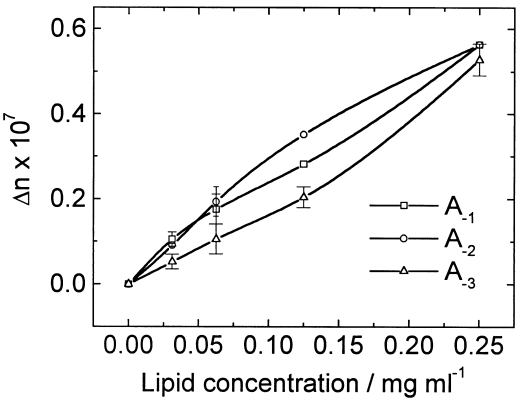

Fig. 10. Birefringence relaxation amplitudes (A_{-i}) of the field-off processes as a function of the lipid concentration. $E=4$ kV/cm, $\Delta t=4$ ms.

gence signal at $C \geq 0.5$ mg/ml, the DOPC concentration was varied between 3.125×10^{-2} mg ml^{-1} and 0.25 mg ml^{-1}. At constant diameter of the vesicles, increasing their number density reduces the mean center-to-center distance d between the particles.

Lipid concentration/mg ml^{-1}	0.25/8	0.25/4	0.25/2	0.25
$d/10^3$ nm	2.34	1.85	1.47	1.17

For the field-on period, using 4 ms long 4 kV/cm pulses, the steady-state birefringence and the amplitudes A_i are found to increase almost linearly with the lipid concentration (Fig. 8), and the variation of the relaxation times τ_i is shown in Fig. 9.

During the field-off reequilibration, the individual amplitudes A_{-i} increase approximately linearly with the lipid concentration (Fig. 10) that, however, has an appreciable effect only on the rate of the slowest reverse relaxation, i.e., on τ_{-3} (Fig. 11). Especially at the lowest concentrations C investigated, the greater than typical uncertainties in τ_{-3} (Fig. 11) and A_{-3} (Fig. 10) are due to the vanishing magnitude of $\Delta n(t,C)$ measured as $t\rightarrow\infty$, which has the most deleterious effect on the determination of the parameters of the slowest relaxation process.

3.1.5. Effects of vesicle size

Vesicles of mean hydrodynamic diameter $\langle D_h\rangle = 95$, 120, and 190 nm were prepared using membrane filters of suitable pore sizes (50, 100 and 200 nm, respectively) during extrusion. The mean aggregation number N of the different size liposomes can be estimated from the lipid concentration and the surface area covered (0.7 nm^2) [12] by the head group of a DOPC molecule.

$\langle D_h\rangle$/nm	95	120	190
$N/10^5$	0.8	1.3	3.2

Using 3 ms long 4 kV/cm pulses, the magnitude of the parameters of both the forward (Figs. 12 and 13) and reverse (Figs. 14 and 15) relaxations is found to increase with vesicle size; however, the effect is very small for τ_1 (Fig. 12) and τ_{-1} (Fig. 14).

3.1.6. Effects of ionic strength

The effects of the presence of free ions were examined by comparing the results obtained on vesicles

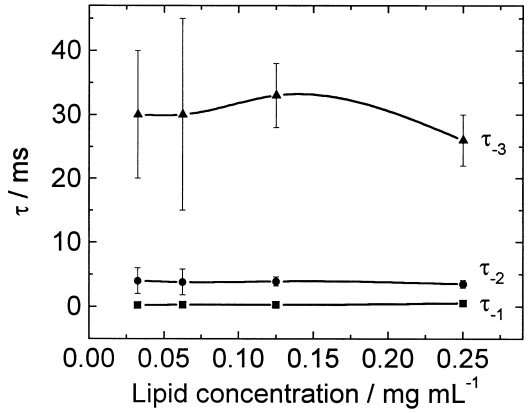

Fig. 11. Birefringence relaxation times τ_{-i} of the field-off processes as a function of the lipid concentration. $E=4$ kV/cm, $\Delta t=4$ ms.

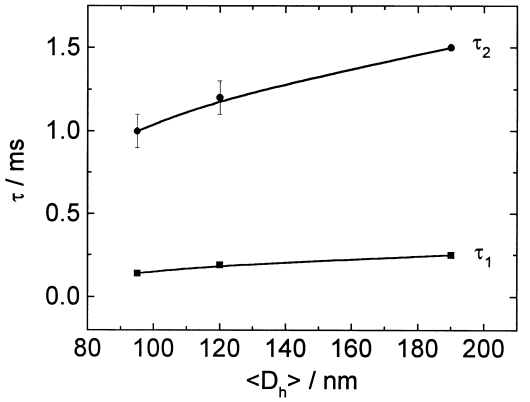

Fig. 12. Birefringence relaxation times τ_i of the field-on processes as a function of the mean hydrodynamic diameter $\langle D_h\rangle$ of the vesicles. $E=4$ kV/cm, $\Delta t=3$ ms.

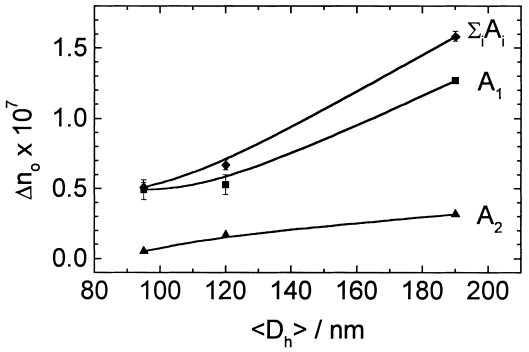

Fig. 13. Steady-state electric birefringence ($\Delta n_o = \Sigma_i A_i$) and birefringence relaxation amplitudes (A_i) of the field-on processes as a function of the mean hydrodynamic diameter $\langle D_h \rangle$ of the vesicles. $E = 4$ kV/cm, $\Delta t = 3$ ms.

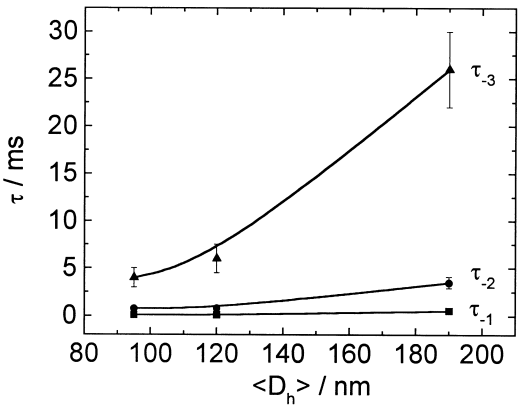

Fig. 14. Birefringence relaxation times τ_{-i} of the field-off processes as a function of the mean hydrodynamic diameter $\langle D_h \rangle$ of the vesicles. $E = 4$ kV/cm, $\Delta t = 3$ ms.

prepared in 10^{-4} M aqueous NaCl with that prepared in pure water. Using 3 ms long 4 kV/cm pulses, the amplitudes of all the forward and reverse processes were found to increase significantly in the presence of the salt, while the relaxation times remained unaffected. The factors by which the amplitudes increase are the following: 1.7 ± 0.03 for A_1, 1.1 ± 0.1 for A_2, 1.6 ± 0.1 for A_{-1}, 1.4 ± 0.08 for A_{-2}, and 1.9 ± 0.2 for A_{-3}.

3.2. Transient induced turbidity

Electric field-induced turbidity of the vesicle solutions becomes detectable only above certain threshold values of the lipid concentration C^*, and the applied field strength E^* and pulse length Δt^*, where, however, each threshold value itself is a function of (inversely proportional to) the applied values of the other two variables, i.e., $C^*(E, \Delta t)$, $E^*(C, \Delta t)$, and $\Delta t^*(C, E)$. Beyond mere detectability, to obtain transient signals with S/N ratio sufficient for the evaluation of the relaxation parameters, the applied conditions must exceed those which correspond to the combination of the thresholds. However, if the threshold conditions are exceeded to a large extent, incomplete and/or anomalous reverse relaxations are observed. A desired balance was achieved by successively reducing the pulse length (in the range of 8–2 ms) when increasing the field strength (in the range of 2–6 kV/cm), and by consistently using high lipid concentrations ($C = 1$–3 mg/ml). In this concentration range, with 190 nm diameter vesicles, their center-to-center distance d is significantly reduced compared to that of the solutions used in the birefringence experiments.

Lipid concentration/mg ml^{-1}	1	2	3
$d/10^3$ nm	0.74	0.59	0.51

At 3 mg/ml, for instance, not more than one vesicle would fit in the average space between two neighboring vesicles.

With the quarter-wave plate and analyzer removed from the detection system (Fig. 2), the evolution of turbidity was monitored via the intensity of the plane polarized laser beam transmitted through the sample. Under exposure to the electric field, the vesicle solution is found to exhibit the polarization properties of a wire-grid polarizer (with the wires running parallel to the applied field ***E***). The transmission axis of

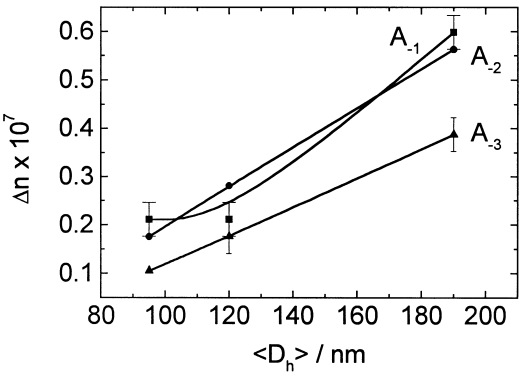

Fig. 15. Birefringence relaxation amplitudes (A_{-i}) of the field-off processes as a function of the mean hydrodynamic diameter $\langle D_h \rangle$ of the vesicles. $E = 4$ kV/cm, $\Delta t = 3$ ms.

the resulting liquid polarizer is perpendicular to $\boldsymbol{E}$. Consequently, under the field ($E = 4$ kV/cm, $\Delta t = 3$ ms), the transmitted intensity $\Delta S_{\parallel}(t)$ of a probe beam polarized parallel to $\boldsymbol{E}$ is decreasing (Fig. 16), while the transmitted intensity $\Delta S_{\perp}(t)$ of a probe beam polarized perpendicular to $\boldsymbol{E}$ is increasing (Fig. 17). The latter case is an example of 'negative turbidity'.

3.2.1. General features of transient turbidity

The field-on and field-off portions of the turbidity relaxation signals cannot be satisfactorily described by multiexponential functions. In attempts to fit single, double or triple exponentials to the data, χ^2 was generally found to be of the order of 10^{-1}. Thus, only the trends in overall amplitude ($A_{\parallel}$ and $A_{\perp}$) and *characteristic* time ($\tau_{\parallel}$ and $\tau_{\perp}$) of the signals $\Delta S_{\parallel}(t)$ and $\Delta S_{\perp}(t)$ can be reported as a function of the experimental variables. Generally, the absolute value of $A_{\parallel}$ is greater than $A_{\perp}$ by a factor of 2–5, with the corresponding signals recorded under identical sensitivity.

3.2.2. The 'parallel' signal $\Delta S_{\parallel}(t)$

The transient turbidity was investigated for lipid concentrations $C = 1$, 2, and 3 mg/ml at 25°C, with applied field strengths of $E = 2$, 4, and 6 kV/cm. Although not exponential in nature, the field-on portion of the signal $\Delta S_{\parallel}(t)$ clearly reveals the presence of at least two processes of disparate rates which contribute to the observed turbidity (Fig. 16a). The associated characteristic times $\tau_{\parallel 1}$ (in the range of approx. 250 to approx. 750 μs) and $\tau_{\parallel 2}$ (in the range of approx. 700 μs to approx. 2 ms) can be estimated from the initial and final slopes of the field-on signal. The rate of both processes increases approximately linearly with E, but is independent of the concentration within experimental error. Also, the corresponding overall signal amplitude $A_{\parallel}$ is found to increase approximately linearly both with the applied field strength and the lipid concentration. The effect of temperature (15, 25, and 35°C) was investigated for a solution of 1 mg/ml concentration using 4 kV/cm pulses. The characteristic time $\tau_{\parallel 1}$ was found independent, whereas $\tau_{\parallel 2}$ was found to slightly increase (from 1.2 ms at 15°C to 1.9 ms at 35°C) linearly with the temperature.

After termination of the pulse, the field-off relaxation involves at least three processes: (i) a fast one in which almost the entire original transmitted light intensity is recovered within approx. 3 ms; (ii) a much slower process for which the signal falls below the baseline (Fig. 16b), but then (iii) it asymptotically returns within a few seconds to the level corresponding to the original equilibrium (not shown in Fig. 16b).

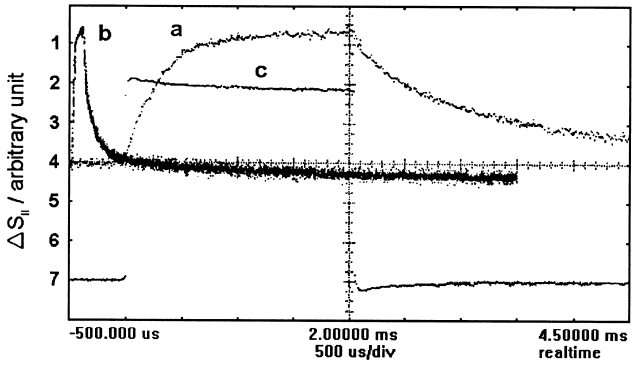

Fig. 16. Oscilloscope traces of the transmitted light intensity change $\Delta S_{\parallel}(t)$ due to field-induced turbidity (a,b) and the attenuated square pulse (c). The probe beam is polarized parallel to E. Time scales: (a,c) 500 μs/div; (b) 10 ms/div. Lipid concentration = 2 mg/ml; $E = 6$ kV/cm; $\Delta t = 2$ ms. Trace b is the display on a slower time scale of all the data points stored for signal a. Subsequently, as established through autotriggering, signal b ascends to the baseline in a few seconds (not shown).

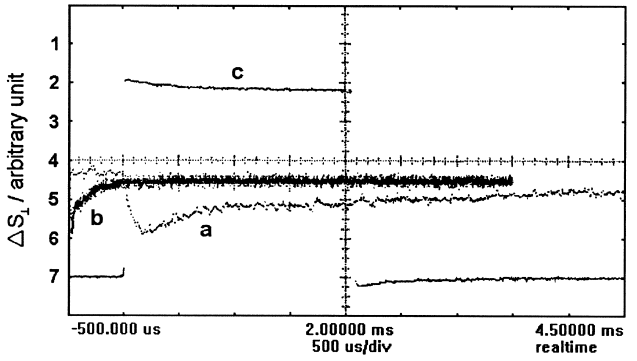

Fig. 17. Oscilloscope traces of the transmitted light intensity change $\Delta S_{\perp}(t)$ due to field-induced turbidity (a,b) and the attenuated square pulse (c). The probe beam is polarized perpendicular to E. Time scales: (a,c) 500 μs/div; (b) 10 ms/div. Lipid concentration = 2 mg/ml; $E = 6$ kV/cm; $\Delta t = 2$ ms. Trace b is the display on a slower time scale of all the data points stored for signal a. Subsequently, as established through autotriggering, signal b ascends to the base line in a few seconds (not shown).

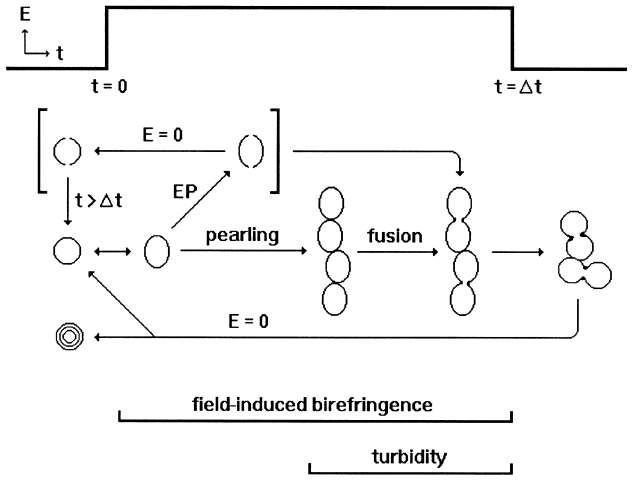

Fig. 18. Schematic representation of the electric field-induced processes in DOPC vesicles, relative to the perturbation square pulse. The double arrow (↔) indicates reversible process with respect to the presence/absence of the field. Electroporation (EP) and its direct products (in brackets) cannot be discerned through birefringence or turbidity. Turbidity (concomitant to birefringence) becomes detectable only at high lipid concentration *and* above certain threshold values of the applied field strength E and pulse length Δt.

3.2.3. The 'perpendicular' signal $\Delta S_{\perp}(t)$

The field-on portion of the signal $\Delta S_{\perp}(t)$ exhibits a minimum (i.e., a maximum in transmitted light intensity) within the period of the perturbation pulse (Fig. 17a), and continues to rise without a break (at the trailing edge of the square pulse) toward the baseline (Fig. 17b), which is reached within a few seconds (not shown).

4. Discussion

4.1. Processes under the electric field

The primary effect of the field applied to the vesicle is the electronic polarization of all constituents of the system, which alone would lead to a small rise of birefringence on the picosecond timescale or faster. With the given limitations of our instrument (maximum field strength, time resolution, and sensitivity), birefringence due to electronic polarization cannot be detected. Neither can the possible birefringence arising from the rotational alignment of small permanent dipoles (i.e., the dipolar head groups of the lipid molecules on the exterior and interior surfaces in the equatorial zone of the vesicle) be seen. This rotational relaxation of the head groups, however, is evident from time domain dielectric spectroscopy (TDDS) measurements on our system, yielding $\tau_r \approx 1$ ns for the process [13]. In the absence of free ions, a possible contribution to birefringence by Maxwell-Wagner polarization can also be discounted, although interfacial polarization can be detected by TDDS in the presence of 5×10^{-3} M NaCl ($\tau_{MW} \approx 160$ ns) [13]. Thus, the induced birefringence observed on the microsecond timescale (τ_1 in Figs. 5,9 and 12) may be attributed to the following processes:

1. the elongation of the time average spherical shell to a prolate ellipsoid (with its major axis parallel to $\boldsymbol{E}$), and possibly the electrostrictive thinning of the membrane in the polar regions of the ellipsoid [5];
2. the rotational alignment of the induced dipolar vesicles parallel to $\boldsymbol{E}$ [6];
3. the rotational alignment of the instantaneously dipolar liposomes. This may arise from asymmetric thermal shape fluctuation of a spheroid shell which leads to an *instantaneous* multipole moment, or a resultant instantaneous dipole moment. The ensuing reorientation by the field may occur through a solid rotation or/and a peristaltic rotation [2,4].

Although each of these processes would contribute to the structural anisotropy of the solution, the electromechanical elongation of the vesicle in the direction of the field seems to play a dominant role. This is suggested by our cumulative results, including the observed maximum in the τ_1 vs. E curve (Fig. 5), which is in qualitative agreement with the prediction of a theory that has been put forward to model the dynamics of electric field induced deformation of lipid vesicles [14]. As reflected in the corresponding birefringence amplitude A_1, the extent of elongation increases with vesicle size (Fig. 13), and if free ions are added to the solution (Section 3.1.6). However, the rate of elongation (τ_1), which is expected to be governed by the bending elasticity κ of the membrane, remains essentially unaffected by vesicle size and ionic strength (Fig. 12 and Section 3.1.6, respectively). Naturally, the birefringence amplitude A_1 in-

creases with the number density of liposomes (Fig. 8), but τ_1 stays largely unchanged (Fig. 9).

It should be mentioned that the early events under the influence of the electric field also include electroporation of the bilayer (Fig. 18), provided the applied field strength is in the 4–8 kV/cm range. Namely, subsequent to the onset of elongation of DOPC vesicles, electroporation could be detected via pore-mediated electron-transfer [15] and precipitation [16] reactions of ionic reactants, the presence of which amounted to an ionic strength of 1.7×10^{-4} to 5×10^{-3} M. Those studies revealed that above threshold values of the applied pulse length Δt, pores of 2.64 Å and approx. 9.6 Å radii appear with a delay of approx. 30 μs and approx. 200 μs, respectively, relative to the onset of birefringence. Although no direct comparison can be made with the present systems of zero ionic strength, the possibility of electroporation exists also under such condition, if the applied field strength is sufficiently high. Formation of the electropores, however, cannot be discerned from monitoring the birefringence or turbidity.

Interaction between the partially aligned induced-dipolar liposomes leads to their vectorial clustering to linear chains (pearling), and to the growth of the chains in the direction of $\boldsymbol{E}$. The resulting increase in structural anisotropy (beyond that due to vesicle elongation) is reflected in a further rise of the birefringence. The slower field-on relaxation associated with τ_2 (Fig. 5) and A_2 (Fig. 4) can be assigned to these processes. This assignment is in accord with the non-monotonic concentration dependence of τ_2 (Fig. 9) which shows a rate initially increasing with the vesicle concentration (up to about 0.15 mg ml^{-1}), as expected for an association process in dilute solution. Above the vesicle concentration 0.15 mg ml^{-1}, the ensuing slow-down may reflect crowding effects which should hamper the formation of linearly oriented chains. In addition, the measured birefringence relaxation time (τ_2 approx. 1 ms) falls in the range of characteristic times $\tau_{\parallel}$ (approx. 250 to approx. 2 ms) obtained from the 'parallel' turbidity signals $\Delta S_{\parallel}(t)$ that, in part, directly report on the formation of oriented linear objects. Interestingly, with increasing field strength applied, the relative contributions of elongation (A_1) and pearling (A_2) to the steady-state birefringence ($\Delta n_o = \Sigma_i A_i$) are reversed at around 2.5 kV/cm (Fig. 4). At low field strength (up to about 1.5 kV/cm), the extent of elongation is small, and the slower pearling is the major source of the birefringence. Above 2.5 kV/cm, however, the effect of elongation becomes dominant.

Under extreme conditions, i.e., above threshold values of the lipid concentration C^*, field strength E^*, and pulse length Δt^* (Section 3.2), the extent of pearling and the degree of fusion of adjacent vesicles within the linear chains reach a level that permits the evolution of the resulting structures to be detected through turbidity. The course and sign of the turbidity signals $\Delta S_{\parallel}(t)$ (Fig. 16) and $\Delta S_{\perp}(t)$ (Fig. 17) reflect the formation of a large number of linear objects oriented parallel with $\boldsymbol{E}$. The maximum exhibited by $\Delta S_{\perp}(t)$ during the perturbation pulse (Fig. 17a) may signal the occurrence of extensive fusion of vesicles (i.e., the formation of a channel between two adjoining bilayer shells) within the linear chains. Fig. 18 provides a schematic summary of the field-induced processes.

4.2. Field-free reverse processes

After termination of the square pulse, the three processes (τ_{-1}, τ_{-2}, and τ_{-3}) associated with the decay of the birefringence reflect the reequilibration of the system, during which the structural anisotropy is destroyed. Due to the absence of the external force, the relaxations involved are significantly slower than those of the field-on processes. Beyond this obvious dissymmetry, the number of relaxations are also different, and the system in the absence of the field ($E=0$) generally cannot backtrack the identical path previously established under the field (Fig. 18).

As far as the birefringence is concerned, the initial state for the reverse relaxations is a structurally anisotropic solution consisting of elongated, intact vesicles (free in the solution, and as constituents of the linear chains), and the linear chains, some segments of which consist of tubular structures (partially fused vesicles). In the fastest relaxation (τ_{-1}), the vesicles are deelongated, i.e., assume their original spherical shape. The rate of the process (τ_{-1}) is independent of the previously applied field strength E (Fig. 7), lipid concentration (Fig. 11), and vesicle size (Fig. 14). The magnitude of the associated amplitude A_{-1} is smaller (Fig. 6) than that of A_1 found for

elongation (Fig. 4). The loss of amplitude indicates that during the later part of the field-on period a portion of the elongated vesicles was incorporated in other structures (through pearling and fusion) within which they can no longer readily relax back to spherical shape after the field is removed. In other words, free liposomes are consumed by pearling/fusion and, hence, only a reduced number of them is left for the fast deelongation process.

The second field-off process (τ_{-2}) can be attributed to the diminishing of the structural anisotropy by kinking and deaggregation of the linear chains. The associated rate is slightly dependent on vesicle size (Fig. 14) and on the previously applied field strength E (Fig. 7), but is independent of lipid concentration (Fig. 11). The observed relaxation time τ_{-2} is also in approximate agreement with theoretical estimates of the rotational relaxation time τ_r of linear vesicle-trimers, if assumed to rotate as rigid rods. However, the observed concentration independence of τ_{-2} (Fig. 11) renders the validity of such an assignment as unlikely.

The reapportionment of the steady-state birefringence Δn_o to the individual field-off relaxation amplitudes A_{-i} entails a significant allotment (A_{-3}) for the slowest reverse process (τ_{-3}) that we attribute to the structural reequilibration and rotation of the fused segments of the linear chains. Under moderate conditions, where only induced birefringence can be observed, the reequilibration leads back to the original system that was present prior to perturbation. This assessment is suggested by light scattering experiments which report the same scattering intensity and size distribution before and after application of the high-voltage square pulse. The details of the reequilibration process are unclear at present, although some hints are provided by the strong dependence of τ_{-3} on the *previously* applied field strength (Fig. 7). Evidently, the memory of the system of the past E must reside in the nature, and the extent of formation, of structures that were created by the end of the pulse, which represent the initial state for the field-off relaxations. Apparently, the original vesicles can be recreated (unfused) faster from structures that resulted at higher fields than from those resulted at lower fields (Fig. 7).

Under extreme conditions, where turbidity is detectable (Section 3.2), the overall reequilibration is much slower (in the seconds range) than that observed through birefringence under moderate conditions. Under extreme conditions, vesicle fusion and other related structural changes are much more extensive, and the liposomes may suffer long lasting, or even permanent, damage – partly as a consequence of the thermodynamic metastability of most unilamellar vesicles [17]. The possibility of the formation of multilamellar vesicles during reequilibration (Fig. 18) is suggested by results of light scattering experiments on the final system, which reveal an unaltered size distribution but a reduced scattering intensity, relative to that of the original system. The suggestion is based on the expected reduction in scattering intensity by the increased density of spherical particles whose radius is comparable to the wavelength of the light [18].

Acknowledgements

This work was supported in part by the National Science Foundation, the Welch Foundation, the donors of Petroleum Research Fund administered by the American Chemical Society, and the Texas Advanced Research Program. The authors thank W. Cook, T. Leeds, and M.W. Lutes for technical assistance.

References

[1] V. Degiorgio, M. Corti (Eds.), Physics of Amphiphiles: Micelles, Vesicles and Microemulsions, North-Holland, Amsterdam, 1985.
[2] Z.A. Schelly, Curr. Opin. Colloid Interface Sci. 2 (1997) 37–41.
[3] E. Neumann, A.E. Sowers, C.A. Jordan (Eds.), Electroporation and Electrofusion in Cell Biology, Plenum, New York, 1989.
[4] E. Tekle, M. Ueda, Z.A. Schelly, J. Phys. Chem. 93 (1989) 5966–5969.
[5] C.T. O'Konski, in: G. Blauer, H. Sund (Eds.), Transport by Proteins, FEBS Symp. 58, Konstanz, 9–15 July 1978, W. de Gruyter, Berlin, 1978, p. 237.
[6] G. Ruderman, B.R. Jennings, R.T. Dean, Biochim. Biophys. Acta 776 (1984) 60–64.
[7] N. Asgharian, X. Wu, R.L. Meline, B. Derecskei, H. Cheng, Z.A. Schelly, J. Mol. Liq. 72 (1997) 315–322.
[8] L.D. Mayer, M.J. Hope, P.R. Cullis, Biochim. Biophys. Acta 858 (1986) 161–168.

[9] R.N.A.H. Lewis, R.N. McElhaney, in: P. Yeagle (Ed.), The Structure of Biological Membranes, CRC Press, Boca Raton, FL, 1992, p. 92.
[10] M.J. Hope, M.B. Bally, G. Webb, P.R. Cullis, Biochim. Biophys. Acta 812 (1985) 55–65.
[11] E. Frederick, C. Houssier, Electric Dichroism and Electric Birefringence, Clarendon Press, Oxford, 1973.
[12] S.M. Johnson, Biochim. Biophys. Acta 307 (1973) 27–41.
[13] I. Ermolina, Y. Polevaya, Y. Feldman, N. Asgharian, Z.A. Schelly, to be published.
[14] A. Sokirko, V. Pastushenko, S. Svetina, B. Žekš, Bioelectrochem. Bioenerg. 34 (1994) 101–107.
[15] N.M. Correa, Z.A. Schelly, Langmuir 14 (1998) 5802–5805.
[16] N.M. Correa, Z.A. Schelly, J. Phys. Chem. B 102 (1998) 9319–9322.
[17] D.D. Lasic, Liposomes: from Physics to Applications, Elsevier, Amsterdam, 1993.
[18] M. Kerker, in: S. Ross (Symp. Chairman), Chemistry and Physics of Interfaces – II, American Chemical Society, Washington, DC, 1971, pp. 170–186.